Progress In Electromagnetics Research C, Vol. 132, 23–35, 2023

Wideband Circularly Polarized Metasurface Based MIMO Antenna for Midband 5G Applications

Abhilash Achariparambil[1, *], Paulbert Thomas[2], and Aanandan Chandroth[3]

Abstract—This work describes the design and analysis of a four-element wideband circularly polarized (CP) Multiple-Input-Multiple-Output (MIMO) antenna for mid-band 5G utilizations. The proposed MIMO antenna miniaturization is obtained by the implementation of composite right/left-handed (CRLH) transmission line (TL) and loading of octagonal shaped slotted rings inside the antenna ground plane. Further, the circular polarization radiation is obtained due to the sequence arrangement of two CRLH-TL based unit cells of opposite branches, inside a conventional square patch. The intended MIMO antenna encompasses two layers, the layer-1 consists of a four-element CRLH-TL based circularly polarized MIMO antenna placed in side-by-side configuration. The layer-2 consists of 3×3 square-shaped metasurface on one side and an octagonal slotted ring on another side. The combination of two layer results in wider bandwidths of 68.84% (2.21–4.53) and 3 dB axial ratio (AR) bandwidth of 30.4% (3.1–4.21 GHz). Furthermore, the antenna has better than 15.3 dB isolation, a maximum gain of 7.2 dBi at 4.04 GHz, radiation efficiency of more than 65%, and lower envelope correlation coefficient (ECC) values across the whole operating band. Diversity Gain (DG) values are high and near to 10 dB. Total Active Reflection Coefficient (TARC) and Channel Capacity Loss (CCL) values are also very much acceptable. As a result, the suggested four-element MIMO antenna is appropriate for midband 5G utilizations.

1. INTRODUCTION

The wireless industry is currently concentrating on miniaturizing antennas and also on its effective radiative performance. By employing metamaterial (MTM)-based transmission line (TL) technologies, antenna miniaturization with superior antenna attributes in terms of antenna impedance bandwidth (IBW) and radiation performance can be easily accomplished. MTMs are artificially engineered electromagnetic structures that have been purposefully designed to have various unique characteristics not seen in nature [1]. MTMs can be implemented utilizing the composite right/left handed (CRLH) TL [2], epsilon negative transmission line [3], Mu-negative transmission line [4], or resonant approaches such as split-ring resonators, electric-LC (ELC) loadings, etc. Recently, the necessity for high-speed data transmission in current application systems has prompted the development of multiple-input multiple-output (MIMO) antenna systems [5].

There are a plethora of different MIMO antenna designs available today. These antennas work with a four-element planar inverted-F antenna with rectangular slots for mutual coupling reduction [6], eight-element inverted-F antenna with artificial magnetic conductor [7], three-port multi-polarized circular patch antenna [8], four-port self-decoupled antenna pairs [9], tightly arranged antenna pairs without decoupling structure [10], four-port antenna based on vector synthetic mechanism [11], quad element circularly polarised MIMO slot antenna using orthogonal configuration [12], four-port wideband MIMO antenna based on slot loop excitation [13], eight-port MIMO antenna using face-to-face elements [14],

Received 28 December 2022, Accepted 23 March 2023, Scheduled 7 April 2023

* Corresponding author: Abhilash Achariparambil (abhilashap@cusat.ac.in).

[1] Department of Electronics, Cochin University of Science & Technology, Kerala, India. [2] Department of Electronics, The Cochin College, Kerala, India. [3] ACARR, Cochin University of Science & Technology, Kerala, India.

four-Port patch antenna loaded with annular-ring antenna with decoupling mechanism [15], and eight-port and wideband orthogonally arranged dual-antenna pairs with a common radiator [16]. The antennas described above have a narrow IBW, a narrower axial ratio (AR) bandwidth, a lower antenna gain, and a lower radiation efficiency. As a result of these factors, conventional existing antennas are unsuitable for new application systems, particularly mid-band 5G applications.

Mid-band spectrum, which spans from 1 GHz to 6 GHz, is perfect for 5G since it can transport a large amount of data over long distances. The Groupe Speciale Mobile Association (GSMA) says that the band of 3.3 GHz to 3.8 GHz is ideal for 5G networks [24]. This paper investigates a four-element, wideband circular polarization (CP) MIMO antenna suitable for the mid-band 5G applications in the above designated frequency range. The combination of the CRLH-TL based MIMO antenna with a square-shaped unit cell loaded metasurface layer results in antenna minimization and wider bandwidth. Reflector strips placed between unit antennas can enhance the overall isolation [4]. The loading of the octagonal slotted ring inside the ground plane also results in antenna size reduction.

2. SUGGESTED DESIGN & ANTENNA GEOMETRY

2.1. Design of the Intended CRLH-TL Based Single Antenna

Figure 1(a) depicts the schematic representation of a circularly polarized unit antenna based on CRLH-TL. The antenna is developed on an FR4 substrate ($H_1 = 0.8$ mm, $\varepsilon_r = 4.4$). Fig. 1(b) depicts an approximate circuit model of the suggested single antenna mentioned in Fig. 1(a). The radiator uses a

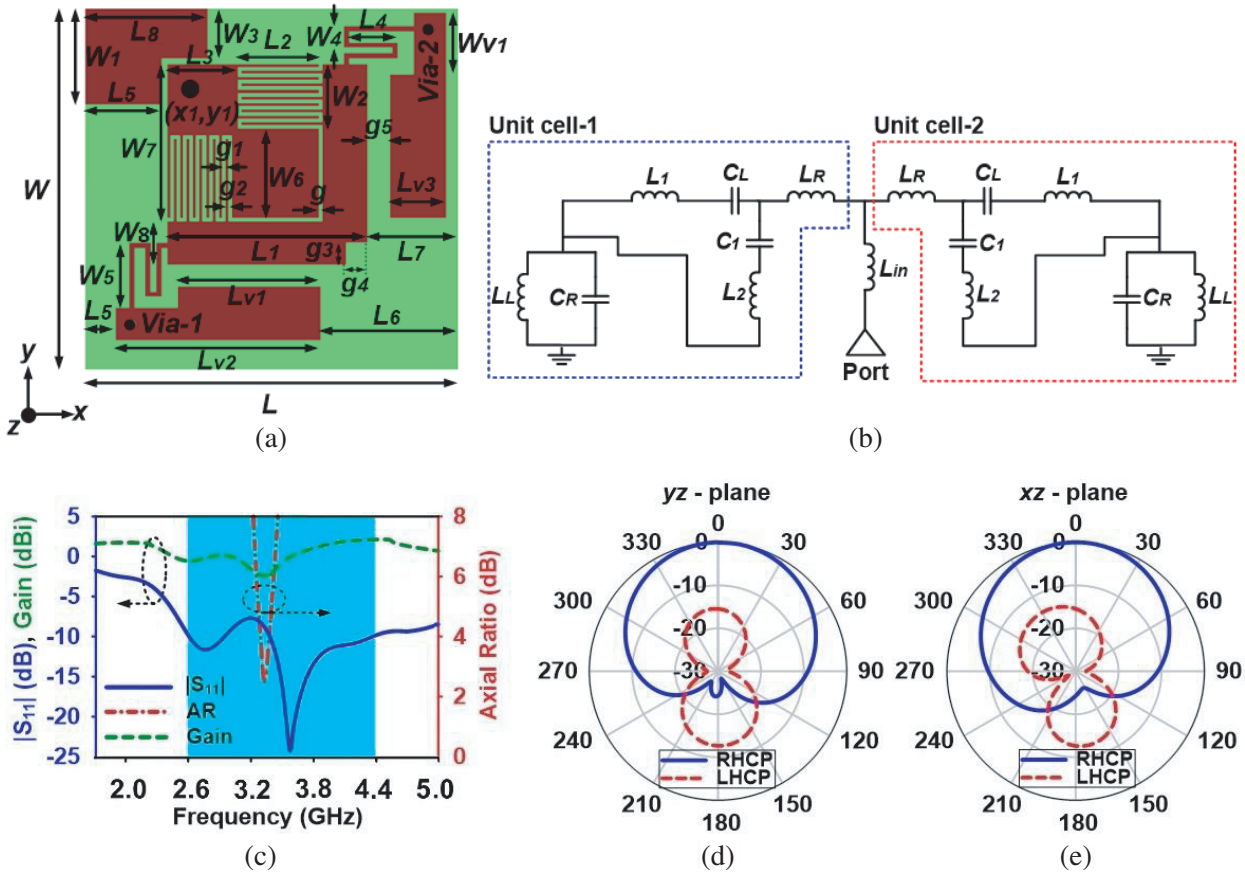

Figure 1. Proposed CRLH-TL based single antenna. (a) Schematic of the single unit antenna, (b) approximate equivalent circuit modelling, (c) reflection coefficient at input ($|S_{11}|$), gain and axial ratio responses, (d) radiation pattern at 3.3 GHz for yz-plane, and (e) radiation pattern at 3.3 GHz for xz-plane.

coaxial feeding technique with feed point represented as (x_1, y_1). Initially, a square patch is designed with length and width being $L_1 = 18.6$ mm. Inside the square patch of single antenna, two CRLH-TL unit cells of opposite branches are loaded to achieve circularly polarized radiation. Thus along the left diagonal of the square patch, two CRLH TLs are positioned as detailed below. Hence by properly optimizing the CRLH-TL elements, a good circularly polarized radiation is obtained with miniaturized antenna size. The antenna can indeed be reduced in size owing to the zeroth-order resonance (ZOR) of CRLH-TL and meandering techniques in the patch [23]. Fig. 2 provides an overview of the developmental stages of the single antenna.

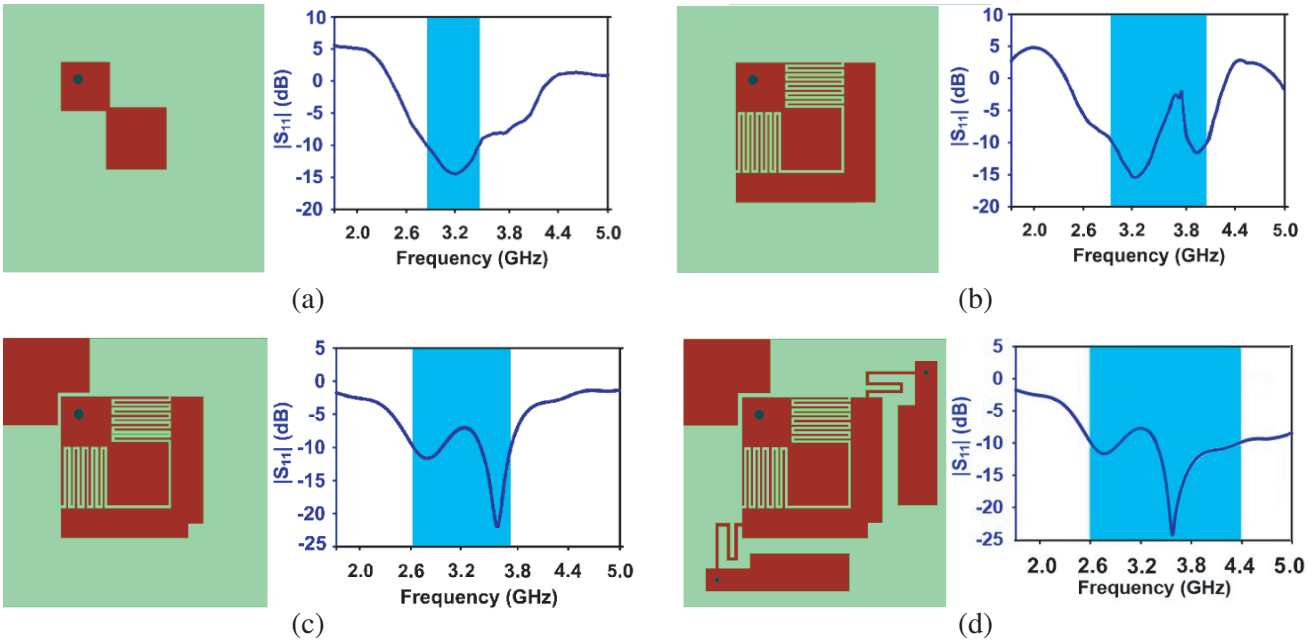

Figure 2. Evolution steps of the unit cell: (a) stage-1, (b) stage-2, (c) stage-3, (d) stage-4 (proposed single antenna).

In the circuit model depicted in Fig. 1(b), for implementing the CRLH-TL concept, the meander line slots of slot width $g_1 = 0.3$ mm provides the series capacitor (C_L) & inductance of L_1. The part of the square patch ($W_6 \times W_6$) offers the series inductor (L_R), and the shorted via of radius $r = 0.3$ mm offers the shunt inductor (L_L). The coupling between upper radiating layer and bottom ground plane offers the shunt capacitor (C_R) of CRLH-TL. The inductor L_{in} represents the inductance of the patch, and C_1 represents the capacitor due to the slot g. The inductor L_2 represents the part of the square shaped patch $L_1 \times W_8$. The parallel arms of L_1-C_L and L_2-C_1 can be reduced to a single LC arm along inductor, L_R forming the series arm of CRLH-TL. Final metrics of the presented single antenna are $L = W = 34.75$, $L_1 = 18.6$, $L_2 = 7.45$, $L_3 = 6.6$, $L_4 = 4.5$, $L_5 = 2.95$, $L_6 = 12.8$, $L_7 = 8.45$, $L_8 = W_1 = 11.5$, $L_{v1} = 13.25$, $L_{v2} = 19$, $L_{v3} = 5.25$, $W_2 = 6$, $W_3 = 5.95$, $W_4 = 2$, $W_5 = 6$, $W_6 = 8.30$, $W_7 = 14.6$, $g = 0.3$, $g_1 = g_2 = 0.3$, $g_3 = g_4 = g_5 = 2$ (All units are in mm).

Figure 1(c) depicts the S_{11}, gain, and axial ratio (AR) responses of the unit element antenna. The circularly polarized antenna offers an impedance BW range beginning with 2.6 GHz to 4.38 GHz (51.02%) and a minimum AR (AR $<$ 3 dB) at 3.3 GHz. Furthermore, at 4.38 GHz, the radiator has a peak gain of 2.5 dBi. The radiator has a gain greater than -2.4 dBi across the whole band. Two-dimensional radiation pattern for the two primary planes yz and xz, computed using microwave CST simulations at 3.3 GHz are illustrated in Figs. 1(d) and (e). Right handed circularly polarized radiation is seen emanating from the unit antenna when being viewed in the direction of maximal radiation, with a front-to-back ratio of 12 dB at 3.3 GHz. The metallic vias with inductive shunt effects are used to visually enlarge radiating patch dimensions, so they present a significant improvement in antenna gain, impedance BW, and axial ratio.

2.2. Design of the 3 × 3 Unit Cell Loaded Metasurface Layer

The antenna mentioned in the preceding subsection does not fulfil the requirements needed for the current systems. To enhance the antenna performance, a 3×3 square single unit cell loaded metasurface is designed [17]. The designed metasurface is depicted in Fig. 3(a), and the corresponding phase response is depicted in Fig. 3(b). The metasurface delivers a $\pm 90^\circ$ phase response ranging from 3.53 to 4.6 GHz. Metasurface improves antenna radiation performance, notably bandwidth, gain, and MIMO isolation. The metasurface provides additional resonance due to surface wave propagation, enhancing performance of the antenna. The stacking of CRLH-TL based circularly polarized antenna and metasurface provides enhanced radiation performance [21]. As portrayed in Fig. 4(c), the metasurface is delineated on an FR-4 substrate with dimensions $H_2 = 3.2\,\text{mm}$, $\varepsilon_r = 4.4$, and $\tan\delta = 0.02$. The measurements have been optimised to $M_1 = 7.5\,\text{mm}$, $M_2 = 7.5\,\text{mm}$, and $g_9 = 0.4\,\text{mm}$.

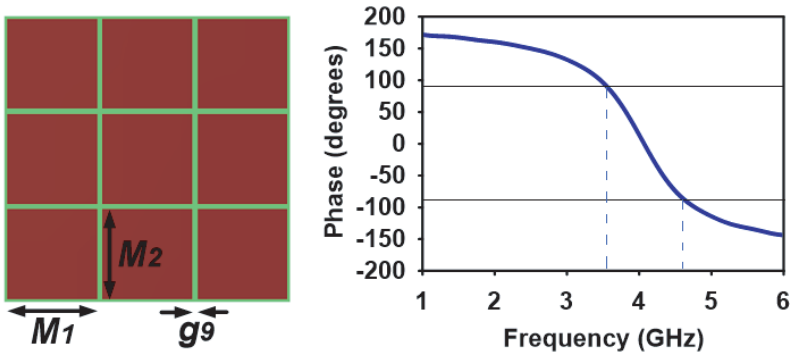

(a) (b)

Figure 3. Square-shaped 3 × 3 unit cell loaded metasurface design. (a) Schematic view of the metasurface, and (b) simulated phase response corresponding to metasurface.

2.3. Design of Four-Port MIMO Antenna with Metasurface

The CRLH-TL-based circularly polarized antenna illustrated in Fig. 1(a) and the 3 × 3 square unit cell loaded metasurface illustrated in Fig. 3(a) are stacked in this section to form a four-port MIMO antenna design. Fig. 4(a) depicts a schematic side sight of a two-layer antenna. Fig. 4(b) illustrates the top sight of the proposed four-element MIMO antenna having four ports (port-1 to port-4).

The separation between metasurface and MIMO antenna structure is critical for better gain and constructive interference between waves emitted by the antenna and those reflected by the metasurface. Multiple simulation experiments have been conducted to determine the optimal distance between the antenna and metasurface while still adhering to the quarter-wavelength standard for maximum gain and isolation between antenna components. The unit antennas are arranged in side by side configuration. Also, isolation structures are placed in between the unit antennas to enhance the antenna isolation. Here the 'I' shaped isolation wall acts like a decoupling structure, and it blocks the incoming electromagnetic waves and thus improves the isolation between individual antenna units. In order to create a novel structure and enhance MIMO performance, this investigation digs deeper into [20] to build the shape of decoupling structure. Fig. 4(c) depicts the metasurface layer of the MIMO antenna. It consists of four unit cell metasurfaces, each placed beneath individual unit antennas. Fig. 4(d) depicts the backside of the metasurface layer, i.e., the ground plane. Here four octagon-shaped rings are placed to improve the antenna performance further. Figs. 4(e) and (f) show the top and bottom views of the fabricated MIMO antenna. The optimized antenna dimensions are $L_m = W_m = 72$, $L_{m1} = W_{m1} = 34.75$, $A_1 = 4.3$, $A_2 = 23$, $A_3 = 7.2$, $A_4 = 14.4$, $M_1 = M_2 = 7.5$, $M_3 = M_4 = 14.7$, $M_5 = 5.35$, $g_6 = g_7 = 3.5$, $g_9 = 0.4$, $B_1 = 9$, $B_2 = 18$, $B_3 = 5.17$ and $S = 0.965$ (All units are in mm).

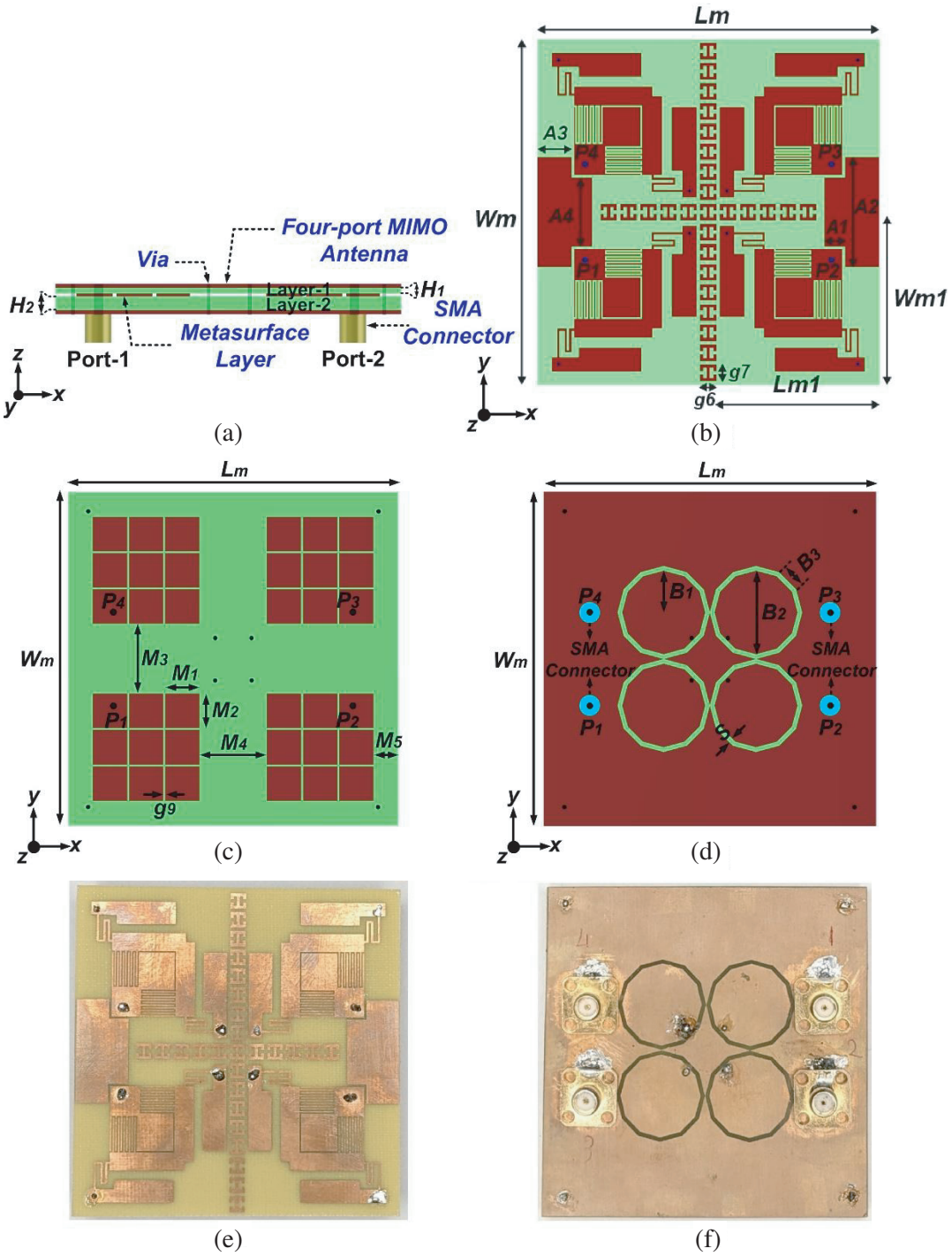

Figure 4. Four-element circularly polarized MIMO antenna. (a) Schematic side sight of four-port MIMO antenna, (b) front sight of layer-1, (c) front sight of layer-2, and (d) back sight of layer-2. [$H_1 = 0.8$ mm, $H_2 = 3.2$ mm]. (e) & (f) Top and Bottom sight of fabricated four port MIMO antenna.

3. MEASURED OUTCOME AND ANALYSIS OF THE MIMO ANTENNA

Figure 5(a) depicts the measured scattering characteristics (S_{11}, S_{12}, S_{13}, and S_{14}) of the projected MIMO antenna. For all ports, the antenna provides a simulated IBW of (2.1–4.51) 72.9% and a measured

IBW of (2.21–4.53) 68.84%. Furthermore, the antenna gives an isolation value greater than 15.3 dB for the suggested antenna. Fig. 5(b) depicts the AR response of the presented MIMO antenna. The antenna has a simulated wide AR bandwidth of 32.1% (3.06–4.23 GHz) and measured AR bandwidth of 30.4% (3.1–4.21 GHz). At 4.04 GHz, antenna gain plots show a maximum simulation gain of 7.5 dBi and measured gain of 7.2 dBi as illustrated in Fig. 5(b). The maximum antenna gain is increased by approximately 5 dBi by changing the single antenna to MIMO antenna with metasurface loaded inside. Furthermore, for the entire band, the radiation efficiency is greater than 65% in the case of MIMO antenna as depicted in Fig. 6. Throughout the operative band, MIMO antenna has got higher efficiency than that of unit antenna.

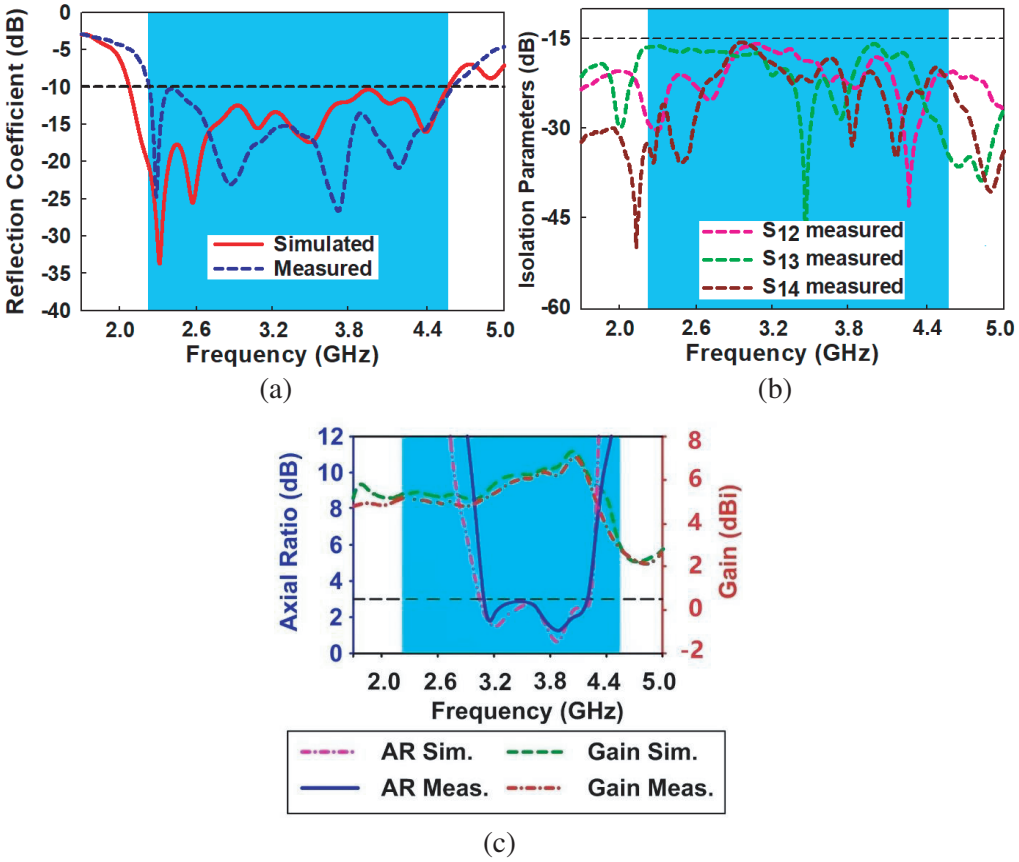

Figure 5. (a) Simulated and measured reflection coefficient, (b) measured isolation parameters, (c) simulated and measured AR and gain response.

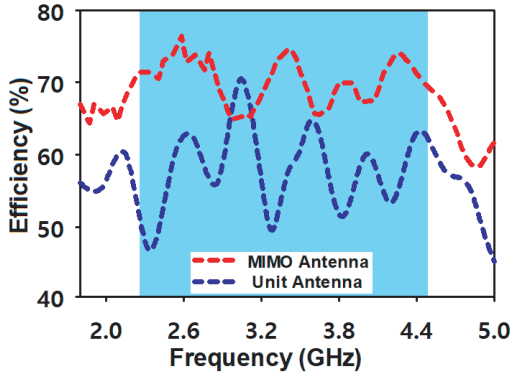

Figure 6. MIMO antenna's efficiency along the bandwidth.

The radiation patterns (simulation and measurement) of the MIMO antenna for port-1 and port-2 at 3.18 GHz (frequency within AR bandwidth of MIMO antenna) are depicted in Figs. 7(a)–(d). Consider Figs. 7(a) and (b), which show that the antenna offers robust right-handed circularly polarized radiation for port-1 for the yz and xz planes. Also in Figs. 5(c) and (d), the antenna provides worthy left-handed circularly polarized radiation for port-2 for the yz and xz planes. Both Right-Hand-Circular-Polarization (RHCP) and Left-Hand-Circular-Polarization (LHCP) are obtained at port 1 and port 2, respectively, due to the side by side arrangement of unit antennas instead of orthogonal arrangement to configure the MIMO antenna.

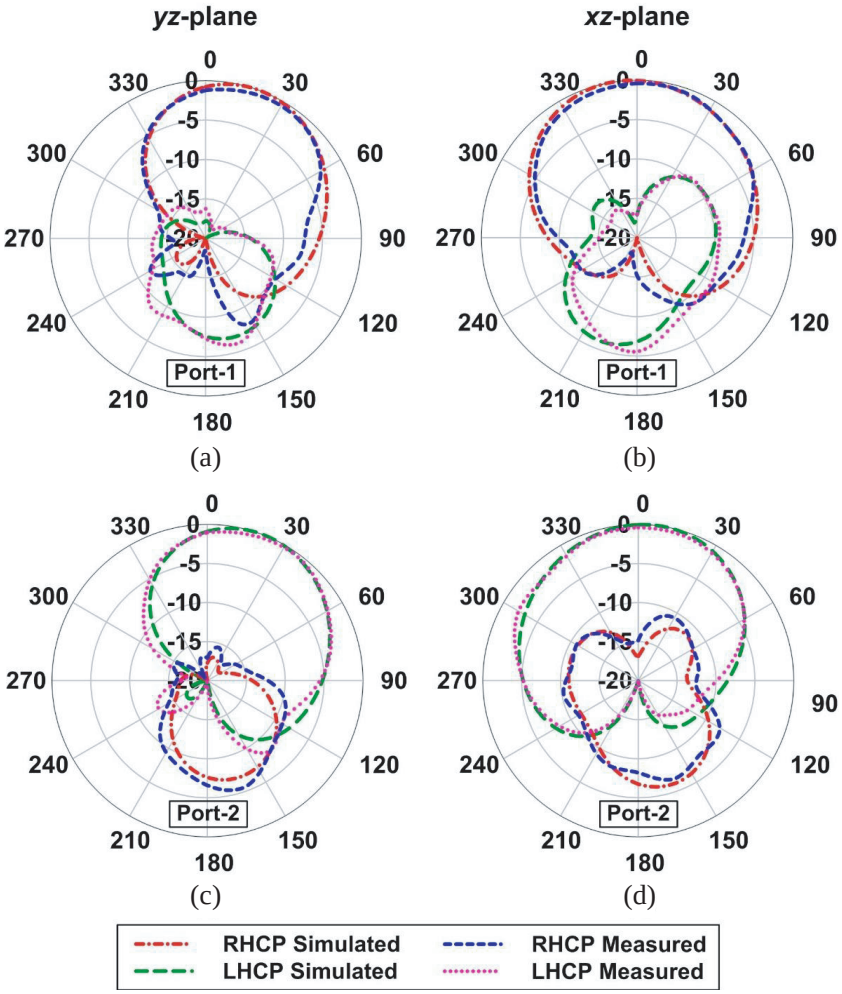

Figure 7. Suggested antenna's simulation and measurement results. (a) Radiation patterns of the MIMO antenna at port-1 for 3.18 GHz in 'yz' plane, (b) radiation patterns of the MIMO antenna at port-1 for 3.18 GHz in 'xz' plane and (c) radiation patterns of the MIMO radiator at port-2 for 3.18 GHz in 'yz' plane, and (d) radiation patterns of the MIMO radiator at port-2 for 3.18 GHz in 'xz' plane.

4. DIVERSITY PERFORMANCE OF THE INTENDED MIMO ANTENNA

For the purpose of explaining the MIMO antenna's behaviour in a multipath fading environment, the diversity performance is computed and analysed. Interference occurs between signals in wireless networks because their pathways require different amounts of time to complete. The close proximity of the unit antennas makes the design of the MIMO system a demanding and formidable task. Because of this close vicinity, the port-couplings and field-couplings both rise. These couplings have an impact on the proposed antenna efficiency and channel capacity [18]. As a result, there is a need for

good isolation and a lesser correlation values. The suggested MIMO antenna's diversity characteristics, such as envelope correlation coefficient (ECC), Diversity Gain (DG), Total Active Reflection Coefficient (TARC), and Channel Capacity Loss (CCL) are determined, as shown in Figs. 8(a)–(d). The performance of the MIMO antenna is assessed by analysing its far-field emission patterns and scattering matrix.

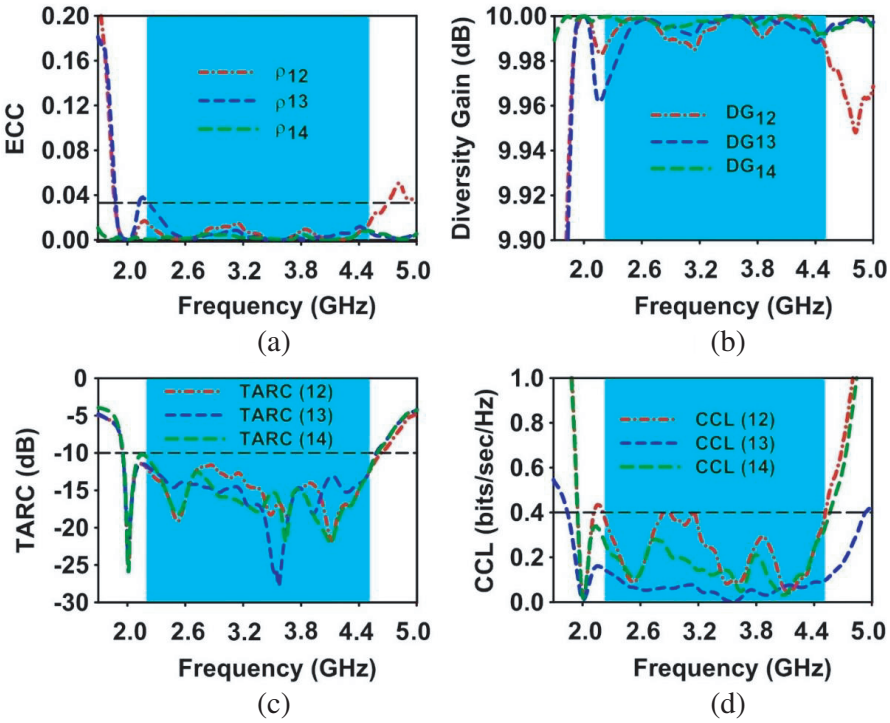

Figure 8. Diversity capabilities of the suggested four port MIMO radiator. (a) ECC, (b) DG, (c) TARC, and (d) CCL.

4.1. Envelope Correlation Coefficient (ECC)

The level of correlation that exists between excited antennas and the other antennas is shown by the ECC. The suggested MIMO antenna's measured ECC (ρ_{12}, ρ_{13}, and ρ_{14}) is represented in Fig. 8(a) using Eq. (1). The measured ECC of the suggested MIMO antenna is less than 0.04 for the whole operative range, indicating good diversity capabilities.

The simulated ECC values are below 0.07 for the complete operational range as seen in Fig. 9. Since ECC values are well below acceptable level of 0.5 [27], it is assured that the unit antennas maintain a degree of independence in their emission patterns.

$$\rho_{ij} = \frac{-S_{ii}S_{ij}^{*} - S_{ji}S_{jj}^{*}}{\sqrt{\left(1-|S_{ii}|^{2}-|S_{ji}|^{2}\right)\left(1-|S_{jj}|^{2}-|S_{ij}|^{2}\right)\eta_i\eta_j}} \tag{1}$$

where 'ρ_{ij}' is the correlation coefficient between antenna elements 'i' and 'j'. 'S_{ij}' is the transmission coefficient between antenna elements 'i' and 'j'. 'η_i' and 'η_j' are the radiation efficiencies of antenna elements 'i' and 'j' correspondingly.

4.2. Diversity Gain (DG)

An improvement in the signal-to-noise ratio brought on by a diversity scheme is known as the diversity gain. The intended MIMO antenna's measured diversity gain plot is displayed in Fig. 6(b), which

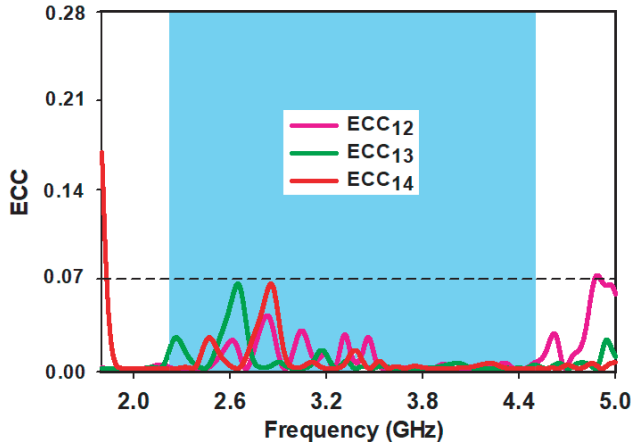

Figure 9. Simulated Envelope Correlation Coefficient between Ports 1, 2 and 3.

was derived using Eq. (2) [19]. According to Fig. 8(b), the developed antenna's Diversity Gain ranges between 9.96 and 9.99, guaranteeing good performance.

$$DG = 10 \times \sqrt{1 - |ECC|} \tag{2}$$

4.3. Total Active Reflection Coefficient (TARC)

TARC is defined as the square root of the ratio of reflected power to incident power. TARC includes the impact of mutual coupling, making it a more relevant and comprehensive characterisation measure of MIMO efficiency. Here, TARC is presented to quantify the frequency range and radiation efficiency of an N-port antenna. The total power at all excitation ports is believed to be incident power. The power transmitted from one port to another is called transferred power, and the power reflected back is called reflected power. According to the results of this multiport study, the frequency bandwidth cannot be estimated by using the scattering parameter or active reflection coefficient (ARC) of a single port, but rather the TARC. For a given port excitation, this method allows one to evaluate the antenna's actual bandwidth [22].

The measured results of TARC between antennas are derived using Eq. (5) and depicted in Fig. 8(c). Fig. 10 shows the calculated TARC with different values of theta [25, 26]. The TARC values are found to be below -10 dB for all phase values.

When the reflected signal is denoted by b_i and the incident signal denoted by a_i, the TARC of a $k \times k$ antenna array can be described as in this way for a given port excitation $[a]$,

$$\Gamma_{\mathbf{a}}^{t} = \frac{\sqrt{\sum_{i=1}^{k} |b_i|^2}}{\sqrt{\sum_{i=1}^{k} |a_i|^2}} \tag{3}$$

The scattering matrix for a 2×2 array of antennas looks like this:

$$\begin{pmatrix} b_1 \\ b_2 \end{pmatrix} = \begin{pmatrix} s_{11} & s_{12} \\ s_{21} & s_{22} \end{pmatrix} \begin{pmatrix} a_1 \\ a_2 \end{pmatrix} \tag{4}$$

The propagation channel is considered to be Gaussian and multipath in MIMO communications. Given that the sum or difference of two independently Gaussian random variables is similarly Gaussian, we may characterize TARC as follows:

$$\Gamma_{\mathbf{a}}^{t} = \sqrt{\frac{|S_{11} + S_{12}e^{j\theta}|^2 + |S_{21} + S_{22}e^{j\theta}|^2}{2}} \tag{5}$$

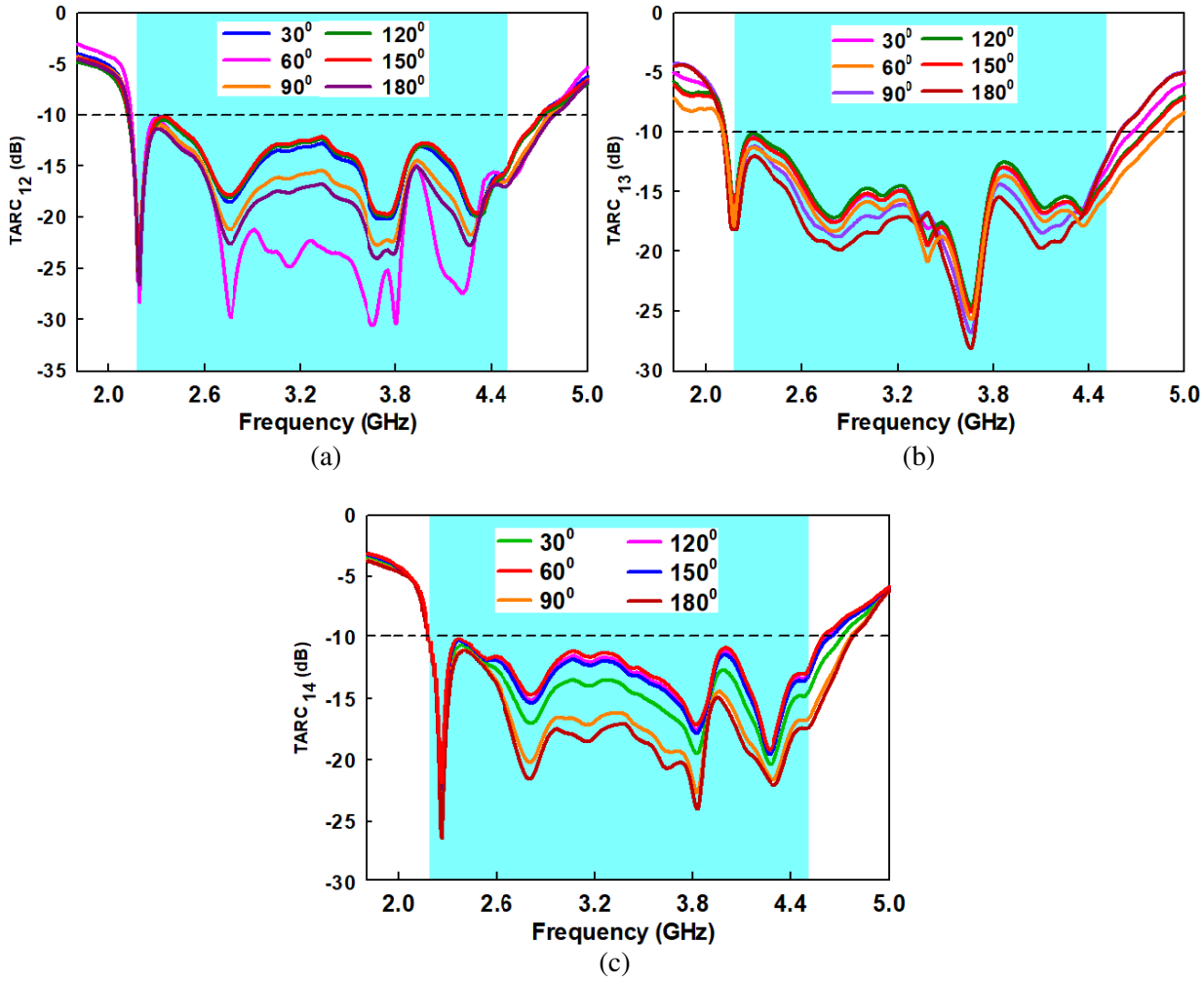

Figure 10. TARC response during phase variation. (a) Between 1 and 2, (b) between 1 and 3, (c) between 1 and 4.

4.4. Channel Capacity Loss (CCL)

The MIMO architecture's channel capacity in independent Rayleigh channels grows linearly with the number of antennas used. On the other hand, the correlation of a wireless channel in the real world could cause the performance of the MIMO design to suffer significantly. According to Fig. 8(d), the suggested four-element MIMO design has an extremely low CCL value [estimated using Eqs. (6) to (8)] below 0.4 bits/s/Hz. The allowed limit of CCL value is 0.4 bits/s/Hz for the operative region [19]. High throughput of the suggested system is ensured by this. CCL, enlisted amongst the MIMO performance characteristics, can be deducted from below:

$$CC_{loss} = -\log_2 \left|\varphi^R\right|, \tag{6}$$

where correlation matrix, $\varphi^R = \begin{bmatrix} \varphi_{11} & \varphi_{12} \\ \varphi_{21} & \varphi_{22} \end{bmatrix}$

$$\varphi_{11} = 1 - \left(|S_{11}|^2 + |S_{12}|^2\right), \quad \varphi_{22} = 1 - \left(|S_{22}|^2 + |S_{21}|^2\right) \tag{7}$$

$$\varphi_{12} = -\left(S_{11}^* S_{12} + S_{21}^* S_{22}\right), \quad \varphi_{21} = -\left(S_{22}^* S_{21} + S_{12}^* S_{11}\right) \tag{8}$$

Table 1 summarizes the improvements in bandwidth, ports, gain, radiation efficiency, and isolation achieved by the proposed quad-element MIMO antenna compared to other conventional compact quad

Table 1. Performance comparison of the suggested MIMO system & various prevailing MIMO systems.

Ref. No.	Electrical Size (λ_0^3)	Ports	Feeding technique	Minimum Isolation (dB)	MIMO Configuration	BW (%)	CP Radiation	AR BW (%)	Gain (dBi)	Rad. Eff.
[6]	$0.52 \times 1.05 \times 0.04$	4	Coaxial feeding	10	Orthogonal	28.5	No	–	≈ 3	NA
[7]	$0.82 \times 1.65 \times 0.01$	8	Probe feeding	10	Orthogonal	12.0	No	–	5	> 50
[8]	$1.87 \times 1.87 \times 0.12$	3	Probe feeding	14	Shared radiator	24.0	No	–	6.6	> 88
[9]	$0.85 \times 1.75 \times 0.08$	4	Microstrip feed	17	Front-to-Front	5.71	No	–	NA	> 58
[10]	$1.75 \times 0.87 \times 0.09$	8	Semirigid cable feeding	17	Front-to-Front	2.71	No	–	NA	> 49
[12]	$0.72 \times 0.72 \times 0.01$	4	Microstrip feed	19	Side-by-side	11.1	Yes	≈ 7	4.5	NA
[13]	$0.42 \times 1.08 \times 0.09$	4	Microstrip feed, coaxial feeding	10	Orthogonal	17.2	No	–	4.5	> 75
[14]	$1.63 \times 0.81 \times 0.05$	8	Coaxial feeding	14	Front-to-Front	10.5	No	–	NA	> 52
[15]	$2.07 \times 2.07 \times 0.16$	4	Coaxial feeding	16.5	Shared radiator	41	No	–	NA	84
[16]	$2.07 \times 1.03 \times 0.11$	8	Microstrip feed	12	Orthogonal	40.9	No	–	NA	> 57.8
This Work	$0.67 \times 0.67 \times 0.03$	**4**	**Coaxial feeding**	**15.3**	**Side-by-side**	**68.84**	**Yes**	**30.4**	**7.2**	**> 65**

element MIMO antenna counterparts stated in references. Compactness, broad bandwidth, circular polarization, good gain, and strong isolation are just a few of the benefits of the proposed quad-element MIMO antenna.

5. CONCLUSION

This paper describes a new approach for increasing Gain, Impedance Bandwidth, and Axial Ratio bandwidth by combining a four-port circularly polarized MIMO antenna with a metasurface layer. To increase the isolation among the individual antenna elements in the MIMO antenna system, an array of reflectors based on a 'I' shaped decoupling circuit was implemented. The MIMO antenna has a higher impedance BW of 68.84% and a higher AR bandwidth of 30.4%. The overall radiation efficiency is better than 65% to the whole operative band. Furthermore, as compared to similar current MIMO designs, the suggested antenna has a smaller size and acceptable gain. The measured ECC of the MIMO antenna is less than 0.04 for the complete usable band. The Diversity Gain is very close to 10 dB ranging from 9.96 to 9.99, which ensures a good performance. TARC values are found to be below -10 dB for the entire operative range. MIMO design has an extremely low CCL value below 0.4 bits/s/Hz for the operative region. As a result, the suggested MIMO antenna is very much relevant for 5G mid-band applications.

ACKNOWLEDGMENT

This work was supported by University Grants Commission's (UGC) research fellowship and the Council of Scientific & Industrial Research's (CSIR) Emeritus Scientist Scheme.

REFERENCES

1. Caloz, C. and T. Itoh, *Electromagnetic Metamaterials: Transmission Line Approach and Microwave Applications*, Wiley, Hoboken, NJ, USA, 2005.
2. Kim, J., "Study on an epsilon-negative zeroth-order resonator antenna properties for mobile handsets," *Microwave and Optical Technology Letters*, Vol. 54, No. 4, 1066–1069, April 2012.
3. Ameen, M. and R. K. Chaudhary, "Electrically small circularly polarized antenna using vialess CRLH-TL and fractals for L-band mobile satellite applications," *Microwave and Optical Technology Letters*, Vol. 62, No. 4, 1686–1696, April 2020.
4. Park, B. and J. Lee, "Omnidirectional circularly polarized antenna utilizing zeroth-order resonance of epsilon negative transmission line," *IEEE Trans. Antennas Propag.*, Vol. 59, No. 7, 2717–2721, July 2011.
5. Singh, H. V., D. V. S. Prasad, S. Tripathi, and A. Mohan, "Closely-coupled wideband MIMO antenna with isolation improvement using decoupling circuit and hexagonal split-ring resonators," *Microwave and Optical Technology Letters*, Vol. 63, No. 10, 2614–2620, October 2021.
6. Chattha, H. T., "4-port 2-element MIMO antenna for 5G portable applications," *IEEE Access*, Vol. 7, 96516–96520, June 2019.
7. Liu, D. Q., H. J. Luo, M. Zhang, H. L. Wen, B. Wang, and J. Wang, "An extremely low-profile wideband MIMO antenna for 5G Smartphones," *IEEE Trans. Antennas Propag.*, Vol. 67, No. 9, 5772–5780, September 2019.
8. Wong, K. L., C. M. Chou, Y. J. Yang, and K. Y. Wang, "Multipolarized wideband circular patch antenna for fifth-generation multi-input-multi-output access-point application," *IEEE Antennas Wireless Propag. Lett.*, Vol. 18, No. 10, 2184–2188, October 2019.
9. Ren, Z., A. Zhao, and S. Wu, "MIMO antenna with compact decoupled antenna pairs for 5G mobile terminals," *IEEE Antennas Wireless Propag. Lett.*, Vol. 18, 1367–1371, July 2019.
10. Sun, L., H. Feng, Y. Li, and Z. Zhang, "Compact 5G MIMO mobile phone antennas with tightly arranged orthogonal-mode pairs," *IEEE Trans. Antennas Propag.*, Vol. 66, No. 11, 6364–6369, November 2018.
11. Huang, H., X. Li, and Y. Liu, "5G MIMO antenna based on vector synthetic mechanism," *IEEE Antennas Wireless Propag. Lett.*, Vol. 17, No. 6, 1052–1055, June 2018.
12. Saxena, S., B. K. Kanaujia, S. Dwari, S. Kumar, H. C. Choi, and K. W. Kim, "Planar four-port dual circularly-polarized MIMO antenna for sub-6 GHz band," *IEEE Access*, Vol. 8, 90779–90791, 2020.
13. Jehangir, S. S. and M. S. Sharawi, "A compact single-layer four-port orthogonally polarized Yagi-like MIMO antenna system," *IEEE Trans. Antennas Propag.*, Vol. 68, No. 8, 6372–6377, August 2020.
14. Xu, Z. and C. Deng, "High-isolated MIMO antenna design based on pattern diversity for 5G mobile terminals," *IEEE Antennas Wireless Propag. Lett.*, Vol. 19, No. 3, 467–471, March 2020.
15. Wong, K. L., J. Z. Chen, and W. Y. Li, "Four-port wideband annular-ring patch antenna generating four decoupled waves for 5G Multi-Input-Multi-Output access points," *IEEE Trans. Antennas Propag.*, Vol. 69, No. 5, 2946–2951, May 2021.
16. Sun, L., Y. Li, Z. Zhang, and Z. Feng, "Wideband 5G MIMO antenna with integrated orthogonal-mode dual-antenna pairs for metal-rimmed smartphones," *IEEE Trans. Antennas Propag.*, Vol. 68, No. 4, 2494–2503, April 2020.
17. Dong, Y., H. Toyao, and T. Itoh, "Design and characterization of miniaturized patch antennas loaded with complementary split-ring resonators," *IEEE Trans. Antennas Propag.*, Vol. 60, No. 2, 772–785, February 2012.

18. Ameen, M., O. Ahmad, and R. K. Chaudhary, "Bandwidth and gain enhancement of triple-band MIMO antenna incorporating metasurface based reflector with for WLAN/WiMAX applications," *IET Microwave, Antennas Propag.*, Vol. 14, No. 13, 1493–1503, October 2020.
19. Abhilash, A. P., K. K. Indhu, R. A. Kumar, K. Neema, and C. Aanandan, "Ultra-wideband quad element MIMO antenna on a flexible substrate for 5G and wearable applications," *Progress In Electromagnetics Research C*, Vol. 126, 143–155, 2022.
20. Yon, H., M. A. Aris, N. H. Abd Rahman, N. A. M. Nasir, and H. Jumaat, "A design of decoupling structure MIMO antenna for mutual coupling reduction in 5G application," *2019 International Symposium on Antennas and Propagation (ISAP)*, 1–3, 2019.
21. Milias, C., R. B. Andersen, P. I. Lazaridis, et al., "Metamaterial-inspired antennas: A review of the state of the art and future design challenges," *IEEE Access*, Vol. 9, 89846–89865, 2021.
22. Manteghi, M. and Y. Rahmat-Samii, "Multiport characteristics of a wide-band cavity backed annular patch antenna for multipolarization operations," *IEEE Trans. Antennas Propag.*, Vol. 53, 466–474, January 2005.
23. Li, Z., Y. Zhu, H. Yang, G. Peng, and X. Liu, "A dual-band omnidirectional circular polarized antenna using composite right/left-handed transmission line with rectangular slits for unmanned aerial vehicle applications," *IEEE Access*, Vol. 8, 100586–100595, 2020.
24. Nokia, "5G spectrum bands explained — Low, mid and high band," https://www.nokia.com/networks/insights/spectrum-bands-5g-world/#:~:text=5G%20mid%2Dband%20spectrum%20provides,GHz%20range%20as%20particularly%20appealing; 2022 [accessed on 10 May 2022].
25. Kumar, A., A. Q. Ansari, B. K. Kanaujia, J. Kishor, and S. Kumar, "An ultra-compact two-port UWB-MIMO antenna with dual band-notched characteristics," *AEU — International Journal of Electronics and Communications*, Vol. 114, Feb. 2020.
26. Wang, F., S. Li, Q. Zhou, and Y.-B. Gong, "Compact wideband quad-element MIMO antenna with reversed S-shaped walls," *Progress In Electromagnetics Research M*, Vol. 78, 193–201, 2019.
27. Ban, Y.-L., C. Li, C.-Y.-D. Sim, G. Wu, and K.-L. Wong, "4G/5G multiple antennas for future multi-mode smartphone applications," *IEEE Access*, Vol. 4, 2981–2988, 2016.